Chalcogenide Letters Vol. 17, No. 6, June 2020, p. 277 - 300

EFFECT OF Se ADDITIVE ON THE STRUCTURE, PRE-CRYSTALLIZATION CRITERIA AND CRYSTALLIZATION KINETIC PARAMETERS IN GLASSY MELT-QUENCHED As-S ALLOY

A. QASEM[a,*], E. R. SHAABAN[b], M. Y. HASSAAN[a], S. RAFIQUE[c],
M. G. MOUSTAFA[a,d], EL S. YOUSEF [e,f]
[a] Physics Department, Faculty of Science, Al-Azhar University, Nasr City 11884, Cairo, Egypt
[b] Physics Department, Faculty of Science, A1-Azhar University, Assiut 71542, Egypt
[c] Multidisciplinary Nanotechnology Centre, College of Engineering, Swansea University, Swansea SA1 8EN, United Kingdom
[d] Physics Department, College of Science & Arts, Jouf University, Qurayat, P. O. 756, Saudi Arabia
[e] Physics Department, Faculty of Science, King Khalid University, P.O. Box 9004, Abha, Saudi P.O. Box 9004, Saudi Arabia Arabia
[f] Research Center for Advanced Materials Science (RCAMS), King Khalid University, Abha 61413,

The present framework is consecrated to studying structural parameters, pre-crystallization criteria and crystallization kinetics by non-isothermal and iso-conversional methods for melt-quenched $As_{40}S_{60-x}Se_x$ glassy alloys, with (x=0, 15, 30, 45 and 60 at. %). Energy dispersive x-ray analysis of the $As_{40}S_{60-x}Se_x$ glassy system appears that the constituent element ratio of the studied samples have been agreed with the nominal compositions. Likewise, Differential Scanning Calorimetry (DSC) and x-ray diffraction (XRD) has been utilized to depict the thermal and structural properties, respectively. Four characteristic temperatures linked to several phenomena are obviously noticed in the studied DSC traces. The first one is T_g that harmonizes with the glass transition temperature. The second one is Tc that harmonizes with the onset of the crystallization temperature. The third one, T_p corresponds to the peak crystallization temperature. The last characteristic temperature, T_p is the melting point. The XRD analysis signalizes to the amorphous structure of the as-prepared glassy alloys. The crystallization kinetics of the powdered of $As_{40}S_{60-x}Se_x$, have been investigated under non-isothermal and iso-conversional conditions. Besides, the values of diverse kinetic parameters such as the activation energy of glass transition, the weight stability criterion, and Avrami exponent, have been computed. The activation energies of the crystallization process of the $As_{40}S_{60-x}Se_x$ glassy alloys were determined by means of classical and also by the iso-conversional methods. The results referred that the rate of crystallization is linked to the thermal stability and glass-forming ability. The kinetic parameters that computed via some classical and isoconversional methods, were found to be dependent on the change of Se content.

(Received March 11, 2020; Accepted June 9, 2020)

Keywords: Structure parameters, $As_{40}S_{60-x}Se_x$ glasses, Thermal stability, Glass-forming ability, Non-isothermal parameters, Isoconversional methods

1. Introduction

Many researchers of physics and several research centers of solid material work extensive research studies on those materials that are based on the chalcogenide elements because of its many uses in the field of modern technology. Chalcogenide materials are utilized for many electronic applications such as IR optical elements, switching devices, optical fibers, optical transmission media, reversible phase change and optical records [1, 2].

---

[*] Corresponding author: alkhteebammar36@yahoo.com

Structure of chalcogenide materials have been extensively studied in binary compositions whether the bulk material or thin film forms. Several binary compounds can be synthesized by associating one of the chalcogen with another element of the periodic table.

Abrikosov and his co-workers [3] were first reported the molecular structures of As-S, As-Se binary glasses according to the phase diagrams for those systems. Thus, As-S glassy alloys can be formed when As element content up to 46%, whereas, the As-Se formed when this maximum content raised to almost 60%. Low As content of glasses can transfer easily to the crystallization materials, for an example, if the As content is 6% , the glass will crystallize at room temperature in short time, namely, almost one day in the range 5-16 weight %, in a couple of days at 60ºC while it takes 30 days for As-S at temperature equals to 280ºC [3] As-Se glassy alloys can crystallize along the all composition range, however this was to be done under pressure and at elevated temperatures.

Ternary chalcogenide glassy alloys also in general studied from more than three decades which can be prepared by insertion a suitable additive element in binary matrix. A ternary As-S-Se system was appeared a very wide glass-forming region [2-8]. The solid solutions can be formed along the line As_2S_3– As_2Se_3 which proved via IR spectra and x-ray analysis by Velinov and his coworkers [9].

As- rich glassy alloys can be formed in several bonds such as As–As, As–Se, and As–S also Se-rich glassy alloys have As–Se, As–S, and Se–Se bonds and finally S-rich glasses As–Se, As–S, and S–S bonds. The main relative weight of each of the above units is expected to be proportionate to the overall composition of the glass itself [10-13].

Chalcogenide glassy alloys are utilized in rewritable optical disks and phase-change memory devices. Using controlling heating and cooling, these compounds can be converted between an amorphous and a crystalline state, herewith changing their optical and also electrical properties and allowing the storage of information and then for these reasons, chalcogenide glassy alloys are very important in modern technique. we try hard to deal with them in all research aspects for the studies as appeared in our published papers [14-16], included the binary and ternary system which consists of As, S and Se elements by a detailed and inclusive way for all the optical, electrical, and even thermal properties. In this work, we will continue to investigate these alloys in order to clarify the structural and thermal properties of them where the knowledge of crystallization kinetic parameters, the glass-forming and also thermal stability, is very important for usage of these glassy alloys in modern technology, in order to assessment their applicability.

The target of the present framework is to compute the structure parameters and analyze the dependence of characteristic temperatures, T_g , T_C , T_P , T_m and the activation energy on the change of Se content of $As_{40}S_{60-x}Se_x$ glassy alloys, with (x=0, 15, 30, 45 and 60 at. %). Also well, the crystallization kinetic parameters corresponding to the crystallization process of the studied glassy alloys and the thermal stability, glass-forming ability, and other thermal criteria are discussed. Structure nature is identified in terms of x-ray diffraction (XRD) measurements, using Cu-Kα radiation and also SEM technique.

2. Experimental methods

The amorphous materials of $As_{40}S_{60-x}Se_x$ glasses, with (x=0, 15, 30, 45 and 60 at. %) were formed by the conventional melt-quenching technique. Highly pure elements, As, S and Se (purchased from Sigma-Aldrich, 99.999%) were weighted accordingly to their atomic percentages, using an electrical balance type (Sartorius) with accuracy ($\pm 10^{-4}$g) and sealed in an evacuated silica tubes (10^{-5} Torr) and it was heated at 1000 c for 32 hours. During the melt process the tube was frequently rocked to intermix the constituents and to increase homogenization of the liquid. On the other hand, the powdered sample was prepared by grinding of the resulting bulk alloy samples in a mortar. The compositional contents of the prepared sample were checked by using the EDAX technique. The percentage ratios of the constituent elements are closed to the measured ratios by electron microprobe analysis. The structure nature of the as-prepared samples was identified by a Phillips X-ray diffractometer. The XRD data were carried out within the range of 2θ=5-75° with a scanning step and speed of 0.02°, and 0.06 °/s, respectively. The X-ray diffractometer composed of Cu K_α radiation source with a graphite monochromator where λ= 1.54178 Å. The crystallization kinetics was monitored by DSC (Model: TA - Q20). For this purpose, ~10 mg of the bulk glass sample was utilized. The measurement was carried out for different compositions ranging and temperature scan ranging from 295 to 575 K. The glass transition temperature (T_g), crystallization extrapolated onset temperature T_C while the crystallization peak temperature are T_P for the exothermic peak and the melting temperature (T_m) were deduced with an accuracy of ±1 K by the microprocessor of the thermal analyzer.

3. Results and discussion

3.1 Elemental and x-ray analysis

The representative EDX spectrum for the studied alloys exhibited the constituent element ratio is near to the nominal compositions where almost: $As_{[40]}$ S $[_{60\text{-}x}]_{\pm0.12}Se_{x\,[\pm0.03]}$. Whereas, XRD patterns of different bulk of $As_{40}S_{60\text{-}x}Se_x$ alloys with (x = 0, 15, 30, 45 and 60 at. %) as demonstrated in Fig. 1. Such figure revealed broad peaks without any sharp crystallization peaks, suggesting that the amorphous nature of such alloys.

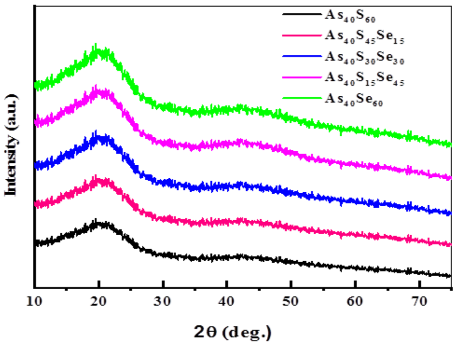

Fig. 1. The XRD patterns of $As_{40}S_{60\text{-}x}Se_x$ *(x = 0, 15, 30, 45 and 60 at. %) alloys.*

3.2. Some structure parameters

3.2.1. The coordination number

To obtain the average atoms coordination with its nearest neighbors of the constituents which called the coordination number ⟨r⟩ [17] for the $As_{40}S_{60\text{-}x}Se_x$ glassy alloys with (x=0, 15, 30, 45 and 60 at. %), from the data of their individual coordination number N^{As}, N^{S}, and N^{Se} which equal to 3, 2 and 2, respectively, we need to apply the subsequence relation [18]:

$$\langle r\rangle = \frac{[(\alpha N^{As}) + (\beta N^{S}) + (\gamma N^{Se})]}{(\alpha + \beta + \gamma)} \tag{1}$$

Here α, β and γ are the concentrations of As, S, and Se, and were proposed to be 40, (60-x) and x at.%, respectively. The all obtained values of $<r>$ for the studied system are 2.4 and this result slightly equals to the value which known as the rigidity percolation threshold (RPT) or an ideal value for glassy alloy. Generally known, in a glass with $\langle r\rangle$ lower than 2.4 is floppy, whereas above 2.4 the structure is over constrained and glass formation becomes difficult.

3.2.2. The number of mechanical constraints

In a glassy system covalent networks constrained mechanically by interatomic valence forces such as , bond stretching constraints, N_α and bond bending constraints, N_β are given by N_α = <r>/2 and N_β =[2 $< r >$ – 3] [19], and equals to 1.2 and 1.8, respectively. The average number of constraints is N_{con}= N_α + N_β, and also can be given by the subsequence form [20]:

$$N_{con} = [5/2 < r > -3] \tag{2}$$

Both the two equations give the same value, namely, the resulted value *of* N_{con} equals to 3 for all the investigated alloys. The value of ($N_{con} = 3$) is named the Maxwell stability criterion for iso-static structures, whereas the networks with $N_{con} \langle 3$ are under constrained (flexible) and with $N_{con} \rangle 3$, they are over constrained.

3.2.3. Role of lone pair electrons

The concept of lone pair in chemistry refers to a pair of valence electrons which are not shared with another atom in a covalent bond [18] and is sometimes named an unshared pair or non-bonding pair. In chalcogenide alloys, the lone pair electrons (L_P) are responsible for the glass formation. It was proposed [18] that the L_P number must be greater than 1 for the ternary system. The number L_P in the present work is determined by the subsequence equation [21]:

$$L_P = V - \langle r \rangle \tag{3}$$

where V is the valence electrons and given from [21]:

$$V = \frac{\{(\alpha.[V]^{As}) + (\beta.[V]^{S}) + (\gamma.[V]^{Se})\}}{(\alpha + \beta + \gamma)} \tag{4}$$

where, $[V]^{As}$, $[V]^{S}$ and $[V]^{Se}$ represent the valence for As, S, and Se elements which equal to 5, 6 and 6, , respectively while α, β and γ are mentioned above. Now, the obtained values of V and L_P for all the investigated alloys are equal to 5.6 and 3.2, respectively. It is observed that the obtained values of L_P for the studied alloys is much greater than 1 (value of L_P for ideal glass in the ternary system), this denotes that $As_{40}S_{60-x}Se_x$ strongly tend to be formed in the amorphous nature.

3.2.4. The deviation of stoichiometry

The deviation of stoichiometry (S_d) is expressed by the ratio of covalent bonding possibilities of chalcogen atom, such as S and Se in the present alloys, to that of a non-chalcogen atom, such as As. The value of S are computed by the subsequence relation [22]:

$$S_d = [\frac{\alpha N^{S} + \beta N^{Se}}{\gamma N^{As}}] \tag{5}$$

For $S_d \rangle 1$, the system is considered as chalcogen-rich and for $S_d \langle 1$ the system is considered chalcogen-poor while at $S_d = 1$, the system is stoichiometry. The obtained values of S_d for all studied alloys equal 9 and hence the investigated glasses belong to the chalcogen-rich type.

3.2.5. The average heat of atomization

The average heat of atomization ($\overline{H}_S$) for the $As_{40}S_{60-x}Se_x$ glassy alloys with (x=0, 15, 30, 45 and 60 at. %), can be evaluated from Eq. (6) [23]:

$$\overline{H}_S = \frac{(\alpha.[H_S]^{As}) + (\beta.[H_S]^{S}) + (\gamma.[H_S]^{Se})}{(\alpha + \beta + \gamma)} \tag{6}$$

The values of heat of atomization of individual elements As, S, Se: 72.37, 66.31 and 54.35 Kcal/mole, respectively [23], and α, β and γ are their respective atomic concentration. The computed values of $\overline{H}_S$, and average single heat of atomization $\overline{H}_S/\langle r\rangle$ decrease with increasing of Se content as shown in Table 1.

Table 1. The average heat of atomization ($\overline{H}_S$), the average single heat of atomization ($\overline{H}_S/\langle r\rangle$), the energies of homonuclear and heteronuclear bonds for the studied alloys.

x at.%	$\bar{H}_S$ [Kcal/mole]	$\bar{H}_S/\langle r\rangle$ [Kcal/mole]	Hetronuclear bonds, $D_{298}[A-B]$ [Kcal/mole]			Homonuclear bonds, $D_{298}[A-A]$ [Kcal/mole]		
			$[As-S]$	$[As-Se]$	$[S-Se]$	$[As-As]$	$[S-S]$	$[Se-Se]$
0	68.73	28.63	98.36	--	--	92.30	101.75	--
15	66.94	27.89		89.54	90.37			79.07
30	65.14	27.14						
45	63.35	26.39						
60	61.55	25.64	--		--		--	

3.2.6. The bond energy

The bond energies for heteronuclear bonds ($D_{(A-B)}$) have been computed using Pauling's relation [24]:

$$[D^{o}_{298}]_{(A-B)} = \sqrt{([D_{(A-A)} * D_{(B-B)}])} + 30(\chi_{\mathrm{A}} - \chi_{\mathrm{B}})^2, \tag{7}$$

where $D_{(A-A)}$ and $D_{(B-B)}$ are the bond energies of the homonuclear bonds, while χ_{A} and χ_{B} are the values of electronegativities of *A* and *B*, respectively. In our work, the χ_{As}, χ_{S} and χ_{Se} equal to 2.18, 2.4 and 2.55, respectively. The number and energy of homonuclear and heteronuclear bonds for the studied compositions are computed according to Eq. (7) and also depending on Random Covalent Network Model (RCNM) and Chemically Ordered Network Model (CONM) models [25-28] and listed in Table 1 and Table 2.

Table 2. The number of yield bonds according to CRN and CON models for the studied alloys.

x at.%	$[As-S]$		$[As-Se]$		$[S-Se]$		$[As-As]$		$[S-S]$		$[Se-Se]$	
	CRNM	*CONM*	*CRNM*	*CONM*	*CRNM*	*CONM*	*CRNM*	*CONM*	*CRNM*	*CONM*	*CRNM*	*CONM*
0	44.51	120	--	--	--	--	30.24	0	19.53	0	--	--
15	45	90	11.93	30	9	0	31.53	0	18	0	4.53	0
30	30	60	28.12	60	10	0	30.94	0	10	0	10.94	0
45	15	30	44.51	90	6.43	0	30.24	0	4.29	0	19.53	0
60	--	--	44.51	120	--	--	30.24	0	--	--	19.53	0

3.2.7. The overall mean bond energy

The overall mean bond energy $\langle E\rangle$ is given by the following relation [29]:

$$\langle E\rangle = E_M + E_R \tag{8}$$

where E_M is the overall contribution towards bond energy arising from strong heteronulear bonds [30] and E_R is the contribution arises from weaker heteronulear bonds that remain after the number of strong bonds becomes maximum [31], and because the value of $S_d \rangle 1$ (see section 3.2.4), namely, the studied system is chalcogen-rich, therefore, the value of E_M is computed from the subsequence relation for the ternary system $As_{40}S_{60-x}Se_x$ glassy alloys with (x=0, 15, 30, 45 and 60 at. %),here also, $\alpha = 40$, $\beta = (60-x)$, $\gamma = x$ and the rest of parameters which find in the next equations have been mentioned in the previous sections:

$$E_M = P_{rich} \times D_{hb} \tag{9}$$

Here P_{rich} is the degree of cross-linking per atoms for chalcogen-rich and is given by:

$$P_{rich} = [\frac{\alpha N^{As} + \beta N^{S}}{(\alpha + \beta + \gamma)}] \tag{10}$$

D_{hb} is the average heteronuclear bond energy and is given by:

$$D_{hb} = [\frac{\alpha N^{As} D(As - Se) + \beta N^{S} D(S - Se)}{\alpha N^{As} + \beta N^{S}}] \tag{11}$$

and

$$E_R = [\frac{2[\left(0.5 < r > - p_{rich}\right) D(Se - Se)]}{< r >}] \tag{12}$$

The values of the overall bond energy, $\langle E \rangle$ are computed according to the equations which previously mentioned and listed in Table 3. One can notice that the behavior of $\langle E \rangle$, identical to the behavior of glass transition temperature, T_g [32]. In our present work both are decreasing with increasing Se content.

Table 3. Some structure parameters and the characteristic temperatures of DSC thermo-gram for the studied alloys.

x at.%	$\langle E \rangle [ev]$	$T_g\|_{Theor.} [K]$	$CE [eV]$	χ	$T_g [K]$	$T_c [K]$	$T_p [K]$	$T_m [K]$
0	136.71	422.38	118.03	2.275	372	416	434	543
15	129.37	399.54	115.39	2.296	362	404	422	532
30	122.03	376.70	112.74	2.317	355	396	414	528
45	114.68	353.87	110.09	2.338	346	385	400	521
60	107.34	331.03	107.45	2.359	336	368	381	509

3.2.8. The theoretical glass transition temperature

The glass transition temperature T_g is the main parameter for description of glassy state. Glass transition temperature can be theoretically calculated using different method [32]. The covalent bond approach (CBO) of Tichy and Ticha [22] may be considered as first approximation in case of glasses. The glass transition temperature is considered to be proportional to mean bond energy, $\langle E \rangle$, which depends upon the factors like coordination number, bond energy and nature of bonds. The correlation between T_g and $\langle E \rangle$ in the form of:

$$T_g\Big|_{Theor.} = 3.11\left[< E > -0.9\right] \tag{13}$$

The theoretical values of T_g are calculated as a function of $< E >$ and presented in Table 3.

3.2.9. The cohesive energy

The cohesive energy (*CE*) is a measure of the chemical stability of the material which is computed via summing the bond energies of all the bonds expected in the material under consideration as shown in Eq. (7) [33]:

$$CE = \frac{\sum (C_i . D_i)}{100} \tag{14}$$

Here C_i is the number of expected chemicals (here, we have been used the yield number according to CONM model) and corresponding bonds which mentioned above in section 3.2.6 and listed in Table 2. D_i is the energy of each bond. The estimated values of *CE,* for investigated compositions decrease with increasing of Se content as shown in Table 3.

3.2.10. The fraction of floppy modes and cross-linking density

Thorpe [34] suggested that there exists a finite fraction of zero frequency normal vibrational modes called floppy modes (*f*). These floppy modes exist in the absence of weaker long-range forces and the fractions of *f* are given by:

$$f = \{(12 - 5 < r >) / 6\}, \tag{15}$$

Using $< r > = 2.4$ for the studied glassy, hence the value of the fraction of floppy modes of all alloys equals to zero. This means that the system has a high rigidity. Moreover, the cross-linking density (X) can be obtained from the subsequence relation:

$$X = (< r > -2). \tag{16}$$

The obtained value of X for the each alloy in investigated system is 0.4. The stability of value cross-linking with increasing of Se content signifies to the stability of rigid regions of networks in the studied alloys.

3.2.11. The electronegativity

The ability of a material to retain its electrons is called the electronegativity. According to principle Sanderson [35], the electronegativity (χ_{GM}) of the studied glassy system has been determined from the subsequence equation:

$$\chi_{GM} \approx \left(\prod_{k=1}^{P} \chi_k \right)^{\frac{1}{P}} \tag{17}$$

Here, the molecule contains *P* atoms (same and/or different) and χ_k, where (k = 1, 2,.., *P*) denote their isolated atom electronegativities. The obtained values of the χ_{GM} for the studied compositions increase with increasing Se content as shown in Table 3. The increase of electronegativity with increasing of selenium content indicates an increase in electron bonding with alloys and thus the increase of the rigidity.

3.3. The thermal analysis of the studied alloys

3.3.1. DSC analysis

In order to studied the crystallization kinetics of melt-quenched $As_{40}S_{60-x}Se_x$ (x=0, 15, 30, 45 and 60 at. %) chalcogenide alloys and confirming their glassy nature, DSC of the powdered of $As_{40}S_{60-x}Se_x$ with at β equals to 5 K/min and in the temperature range, 295-575 K is carried out as present in Fig. 2. It is observed from DSC data, four characteristic phenomena are detected in the investigated temperature range for the all investigated alloys. The first one (T_g) corresponds to the glass transition which associated with absorbing energy to overcome the rigidity of the lattice. The second one T_c corresponds to the onset of the crystallization temperature for crystallization peak. The third one characteristic temperature (T_p) describes the peak crystallization temperature. The last describes temperature (T_m) is the melting point. As mentioned, the DSC thermo-grams reveal a single glass transition and a single exothermic crystallization peak. The values of the characteristic temperatures (T_g ,T_c ,T_p and T_m) of the studied glassy alloys at the mentioned heating rate, β, are estimated from the DSC traces and summarized in Table 3. From Table 3, it is observed those values are shifted to a lower temperature with the increase of Se content and this noticed in our published paper about the same compositions [16] which under study now but the main difference that the study in this framework have been taken from bulk materials whereas the study in our published paper done from the results of sheet resistance on the $As_{40}S_{60-x}Se_x$ (x=0, 15, 30, 45 and 60 at. %) thin films by calculation method without the need to make thermal measurements. This observation confirmed that all these transitions and transformations are thermally ineffectual. The observation of one endothermic peak for the melting phenomena could be attributed to the formation of one phase through the heating which confirmed by the XRD analysis. The existence of a single glass transition temperature reveals that the formed the investigated glasses are more stable than those glasses revealing multi-glass transition temperatures.

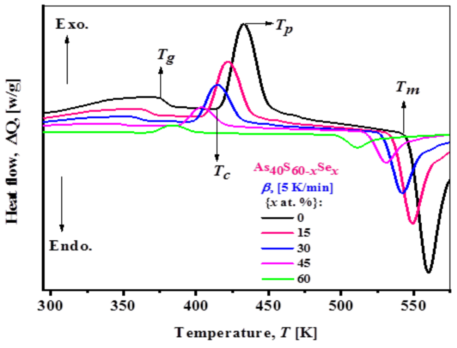

Fig. 2. The DSC tract of $As_{40}S_{60-x}Se_x$ *x = 0, 15, 30, 45 and 60 at. %) alloys at 5 K.min*$^{-1}$.

3.3.2. Thermal stability parameters

There are sundry parameters related the heating by glass stability. According to the nucleation theory, Kauzmann [36] and later Turnbull [37] suggested a classical parameter utilized as a good criterion for glass formation which defined as the ratio between the glass transition temperature, T_g to the melting temperature, T_m , also this parameter is called as reduced glass transition temperature, T_{rg} where ($T_{rg} \geq 2/3$, a good criterion is closed to 1) and generalized by the following equation [37]:

$$T_{rg} = \frac{T_g}{T_m} \tag{18}$$

The ease of glass formation is evaluated by computing the reduced glass transition temperature, T_{rg} based on Eq. (18). The obtained values of T_{rg} are computed and listed in Table 4. It found to be the low of 2/3 increases with the increase Se content, this denotes that bad glass forming ability is for the higher Se content alloy. On the other words, assuming that viscosity is constant at T_g , materials with higher T_{rg} values would be expected to have a higher viscosity between T_g and T_m and consequently be more resistant to crystallization. Thus, the closer the T_{rg} value is to 1, the higher the material's GFA.

Table 4. Thermal stability criteria, the theoretical band gap, $E_g^{opt.}$, and some of kinetics crystallization parameters for studied alloys.

x at.%	T_{rg}	ΔT, $[K]$	S_{p}, $[K]$	H'	H_r	k_H	$E_g^{opt.}$ $[ev]$	$(\frac{d\chi}{dt})_p \times 10^3$ $(\min)^{-1}$	β_w	n		E_c [kcal/mol.]	ΔH_c $[j/g]$
										Eq.30	***Eq.31***		
0	0.685	44	2.12	0.118	0.165	0.346	0.94	2.17	17.33	2.72	3.34	29.47	25.04
15	0.680	42	2.08	0.116	0.163	0.328	0.82	2.11	17.42	2.50	3.14	27.12	16.15
30	0.672	41	2.07	0.115	0.157	0.310	0.73	2.07	17.88	2.36	2.94	26.14	10.84
45	0.664	39	1.69	0.112	0.123	0.286	0.61	2.00	17.55	2.12	2.80	25.61	5.53
60	0.660	32	1.23	0.095	0.101	0.226	0.48	1.91	16.84	1.84	2.65	24.84	1.90

The common criterion utilized also to determine the glass thermal stability against crystallization is Deiztal's criterion, which is defined by the subsequent relation [38]:

$$\Delta T = T_c - T_g \tag{19}$$

The kinetic resistance to crystallization is given by the difference $\Delta T = T_c - T_g$ and this difference represents the thermal stability of the glass [38, 39]. The glassy becomes more stable as ΔT increases. On the other hand, the temperature difference ΔT is a perfect signification of thermal stability because the higher the value of this difference gives higher resistance to crystallization and thus more the retard in various the nucleation processes [39].

The glass alloys with lower ΔT values are expected to have higher electrical conductivity [40, 41]. The obtained values of the thermal stability ΔT for the investigated alloys are computed and summarized in Table 4. The values of, ΔT, decrease (as presented in Table 4 with the increase of Se content. In other words, the thermal stability against crystallization is getting worse with increasing of concentration of Se element in the studied system. Thus, the investigated glassy alloys are less stable whenever the Se content increases.

In the same subject, there are other two criteria give information about thermal stability, which suggested by Saad and Poulain [42]. The first one is called S-parameter (S_P) and the second is called the weighted thermal stability criterion (H'), they are given by the following equations:

$$S_P = [(T_p - T_C) \times \frac{\Delta T}{T_g}]; \; H' = \frac{\Delta T}{T_g} \tag{20}$$

The thermal stability S_P, refers to the resistance to devitrification after the formation of the glass. The difference between T_p, and T_c in Eq. (20), is linked to the rate of devitrification transformation of the glassy phases. The values of S_P and H' for the $As_{40}S_{60-x}Se_x$ glassy alloys with (x=0, 15, 30, 45 and 60 at. %) at the mentioned heating rate are computed for crystallization stage and presented in Table 4. It has been observed that the values of ΔT, the S_P and H' do-follow decreasing trend with an increase of Se content. These combined reasons and all these criteria in crystallization stage are utilized to determine the stability in terms of the change of Se content in the investigated glassy alloys.

3.3.3. Hruby criterion and the glass-formation factor

Hruby's criterion (H_r) which utilized to deduce the thermal stability of the glass via the characteristic temperatures based on the following relation [43]:

$$H_r = \frac{\Delta T}{T_m - T_p}, \tag{21}$$

The parameter H_r gives the probability of obtaining glasses which increases as the difference $T_m - T_p$ decreases and ΔT increases. The obtained values of H_r indicate that the glass-forming is almost difficult because the values of the mentioned parameter are close to 0.1, where if the parameter H_r is less or equal 0,1 , the glass-forming will be difficulted, while good glasses can be formed if the parameter H_r is more or equaling to 0.4 [43].

On the other side, the glass-formation factor or ability parameter (k_H) of the investigated system is expressed by:

$$k_H = \frac{\Delta T}{T_m - T_c} \tag{22}$$

The k_H parameter used as a measure of the glass-forming tendency, for an instant the higher values of criterion parameters reveal the greater thermal stability of the formed glass. The values of all these parameters are estimated for the studied glassy alloys and then summarized in Table 4. Both of these parameters (H_r and k_H) regressive with increasing of the Se content. Thus the ability to the glass-forming is diminished.

3.4. Estimation of optical energy gap

The empirical optical energy gap, E_g can be obtained as a function of the glass transition temperature, T_g from the Shimakawa's equation [44]:

$$E_g^{opt} = 5.11 \times 10^{-3} [\frac{T_g - 298}{\langle r \rangle - 2}] \tag{23}$$

where, ⟨r⟩ is the coordination number which previously mentioned. The computed values decrease and behave the same manner as the glass transition temperature, T_g as shown in Table 4.

3.5. The exothermic heat flow analysis

Fig. 3 shows the exothermic heat flow (ΔQ_{exo}) against temperature (*T*) at (*x*=0 at.%) in the crystallization region, as one example from all studied alloys. In Fig. 3, χ_T is the crystallized fraction at a given *T* expressed by relation $\chi_T = A_T / A$, where *A* is the total area of the peak and A_T is the area of the crystallized part (the area between $T_{on.}$ and a given temperature *T*). Both T_{on} and T_{end} are the initial and final crystallization temperature, respectively.

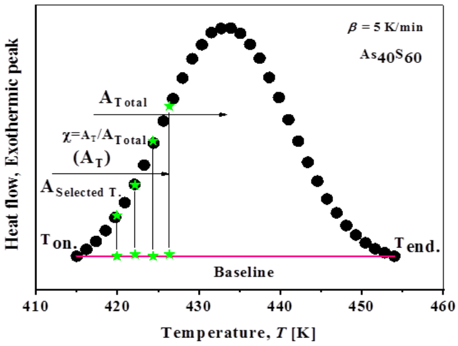

Fig. 3. DSC traces for bulk $As_{40}S_{60}$ glass alloy at 5 $Kmin^{-1}$; for the exothermic peak.

In the same way, the area under the crystallization peak is directly proportional to the total amount of crystallized alloy. The ratio between the selected ordinates and the total area of the exothermic peak shows the corresponding crystallization rates, which make it possible to plot the curves between volume crystallization fraction and temperature.

The experimental graphical of the volume fraction crystallized (χ) appears the typical sigmoid curve as a function of T at different β for the studied system as demonstrated in Fig. 4 and expressed as follows:

$$\chi = \sum_{i=0}^{s} \Delta Q_{exo} \,/\, \sum_{i=0}^{99} \Delta Q_{exo} \tag{24}$$

where s is a number of points of ΔQ_{exo}, (namely, s=0 to 99). According to Eq. (24), the value of χ varies in between 0 and 1 corresponding to a minimum and maximum crystallization fraction, respectively. Three main stages can be distinguished. The stage (1) represents nucleation which occurs at various points in the bulk of the alloy. The stage (2) shows the growth of nuclei with increased rate of reaction as the surface area of nucleation increases. The stage (3) shows the decreases in surface area as a result of nuclei coalescin, the positions of the stages are shown in Fig. 4.

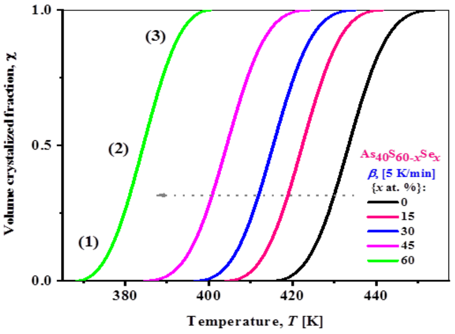

Fig. 4. The typical sigmoid curve of the volume fraction crystallized as a function of temperature, T, for $As_{40}S_{60-x}Se_x$ *(x = 0, 15, 30, 45 and 60 at. %) alloys at 5 K.min*$^{-1}$*.*

Now, the relationship between crystallization rate $({}^{d\chi}\!/_{dt})$ and the temperature produced by differentiating of the volume crystallized fraction as a function of time (t), which given by the subsequence equation for the maximum crystallization rate:

$$\left(\frac{d\chi}{dt}\right)_p = \frac{dT}{dt} \times \left(\frac{d\chi}{dT}\right)_p = \beta \times \left(\frac{d\chi}{dT}\right)_p = \beta \times T_p \tag{25}$$

Figs. 5 represent the crystallization rate $({}^{d\chi}\!/_{dt})$ as a function of temperature for the exothermic crystallization peak. The values of the maximum crystallization rate evaluated using Eq. (25) and listed in Table 4. From Fig. 4 and Fig. 5, one can conclude that the saturation of crystallization shifts towards the lower temperature as the Se content for the investigated glassy alloys increases.

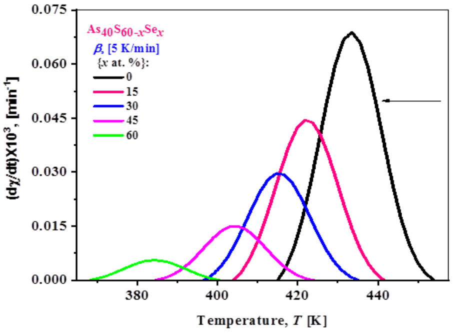

Fig. 5. Crystallization rate versus temperature of the exothermal peak for $As_{40}S_{60-x}Se_x$ *(x = 0, 15, 30, 45 and 60 at. %) alloys at 5 K.min*$^{-1}$*.*

3.6. The glass transition

The apparent activation energy of the glass transition (E_t) of the investigated glassy alloys has been computed by Kissinger's formula [45]:

$$\ln\left(\beta/T_g^{\ 2}\right) = E_t/RT_g + const. \tag{26}$$

Fig. 6 plots the relation between the, $\ln\left(\beta/T_g^{\ 2}\right)$, against 1000/ T_g for the studied chalcogenide glassys. From the slope of the fitted data, the activation energy for the glass transition E_t has been obtained and equaled to 5.87293 kJ/mole (1.40501 kcal/mole) by Kissinger`s formula. The computed value of E_t lie in the range generally observed for other chalcogenide glasses [46, 47, 38].

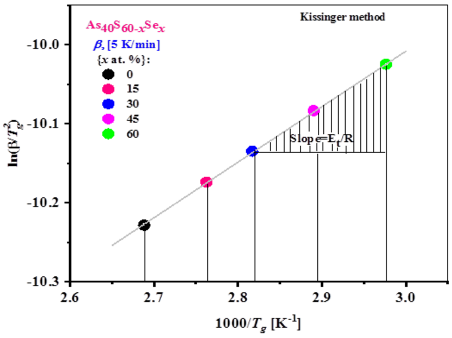

Fig. 6. The plot of $\ln\left(\beta/T_g^{\ 2}\right)$ *verses 1000/* T_g *for* $As_{40}S_{60-x}Se_x$ *(x = 0, 15, 30, 45 and 60 at. %) alloys at 5 K.min*$^{-1}$.

3.7. Fragility index

The liquid fragility is an important parameter that has beneficial as a basis for organizing data on glass-forming liquids and then facilitating the investigation of relaxation processes and glass transition in the super-cooled liquid state. The fragility index (F) can be determined by the subsequent relation [48, 49]:

$$F = \frac{E_t}{RT_g \ln(10)} = \frac{E_t}{2.303RT_g} \tag{27}$$

where E_t is the activation energy for the glass transition that has been estimated according to Kissinger's relation. Fig. 7(a) appears the plot of the liquid fragility, F as a function of $(1000/T_g)$ based on Eq. (27). From this figure, one can note that the value of F increases with the decreasing of T_g.

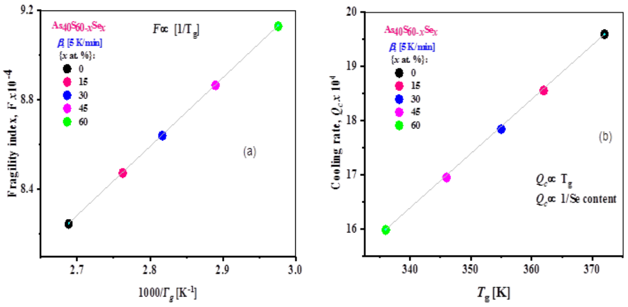

Fig. 7. The plot of the liquid fragility, F versus 1000/ T_g *(a) the plot of the cooling rate, (*Q_c*) as a function of the glass transition temperature,* T_g *(b) for* $As_{40}S_{60-x}Se_x$ *(x = 0, 15, 30, 45 and 60 at. %) alloys at 5 K.min*$^{-1}$.

3.8. The cooling rate

The dependence of the cooling rate (Q_c) on the glass transition temperature measured during cooling obeys the subsequence equation [50- 52]:

$$Q_c = [\frac{RT_g^2}{E_t}] = [\frac{T_g}{2.303F}] \tag{28}$$

The plot of the cooling rate as a function of the glass transition temperature is presented in Fig. 7(b). We note from this figure that the cooling rate has the same behavior of the glass transition temperature.

3.9. The activation energy by non-isothermal methods

The DSC data have been analyzed by several methods to obtaine the activation energy of amorphous-crystalline transformation (E_c), the Avrami exponent (n), the frequency factor (K_0) and the rest constants for the studied glassy alloys.

3.9.1. Kissinger Method

The activation energy of amorphous-crystalline transformation is originally computed utilizing Kissinger's formula [45] as follows:

$$\ln\left(\beta/T_p{}^2\right) = E_c/RT_p - \ln(E_c/RK_0) \tag{29}$$

Fig. 8 shows the plots of $\ln\left(\beta/T_p{}^2\right)$ against $(1000/T_p)$ for the studied system. The plots were found to be straight line. The values for E_c equal to 6.75263 kJ/mole (1.61546 kcal/mole), whereas the value of K_0 equal to $(3.34\times10^{-6})s^{-1}$ for exothermic peak.

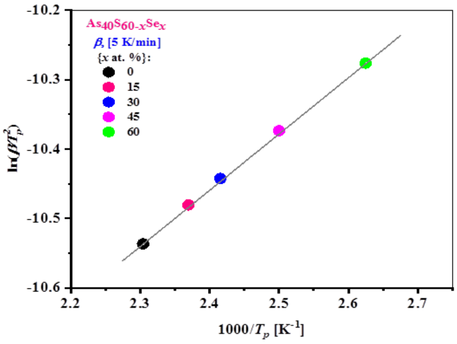

Fig. 8. The plot of $\ln\left(\beta/T_p{}^2\right)$ *versus* $(1000/T_p)$ *for* $As_{40}S_{60-x}Se_x$ *(x = 0, 15, 30, 45 and 60 at. %) alloys at 5 K.min*$^{-1}$*.*

On the other hand, one can compute the kinetic exponent from the experimental values of the $({}^{d\chi}\!/_{dt})_p$ by the subsequence equations:

$$n = \frac{RT_P^2(d\chi/dt)_p}{(37\times10^{-10}).\beta E_c} \tag{30}$$

$$n = (2.5\times10^{-4})\frac{R}{E_c}\frac{T_P^2}{\beta_W} \tag{31}$$

where, β is the heating rate and β_W is the full width at half maximum (FWHM) of the exothermic peak. The values of n for studied glassy alloys are computed and listed in Table 4. The numerical values of the experimental data, T_p, and $(d\chi/dt)_p$, are shown in Table 3 and Table 4, respectively, and the value of the activation energy of crystallization process for the crystallization peak which get from Kissinger method (1.61546 kcal/mole), make it possible to be deduced, through Eq. (27), the kinetic exponent, *n*, for each of the studied samples, whose values are also given in Table 4 have be computed according to the mechanism of crystallization Mahadevan *et al.* [38] which has appeared that *n* may be 4, 3, 2, or which are linked to different glass-crystal transformation mechanisms: (*n* =4, volume nucleation, 3D growth); *(n* =3, volume nucleation, 2D growth), (*n* = 2, volume nucleation, 1D growth); *n* = 1, surface nucleation, one-dimensional growth from surface to the inside. Therefore, bearing in mind the above obtained average values, $\langle n \rangle = 2.31$ based on Eq. (30) and $\langle n \rangle = 2.97$ according to Eq. (31) (as shown in Table. 4) for the crystallization peak, means (volume nucleation, 2 D growth). The computed *n* values are not integers. This means that the crystallization occurs by more than one mechanism [53, 54].

3.9.2. Matusita Method

Furthermore, the activation energy of the studied glassy alloys was computed via the Matustia formula [55]:

$$\ln(-\ln(1-\chi)) = -n \ln \beta - 1.052 \frac{mE_c}{RT} + const. \tag{32}$$

where (*m*=*n*-1) is the dimension order parameter and (*n*) is constant related to the crystallization mechanism. Fig. 9 plots $\ln(-\ln(1-\chi))$ versus $1000/T$ at 5 K/ min. for the studied system. For the computation of E_c we take into consideration the linear region of this plot. From the average *n* values and mE_c ($n=m+1$), the effective activation energies E_c for the studied system are computed and listed in Table 4, where (*n*= 2.97 and *m*=1.97).

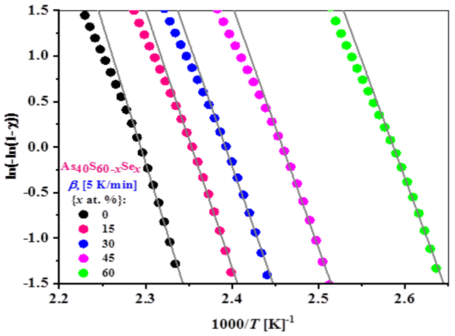

Fig. 9. The plot of $\ln(-\ln(1-\chi))$ *versus (*$1000/T$ *) for* $As_{40}S_{60-x}Se_x$ *(x = 0, 15, 30, 45 and 60 at. %) alloys at 5* $K.min^{-1}$*.*

3.10. Kinetics parameters of the crystallization

According to Surinach *et al.* [56] and Hu and Jiang [57] the thermal stability of glassy materials estimates via two criteria by taking advantage of Arrhenius 's equation as follows:

$$K(T_g) = K_0 \exp[-\frac{E_c}{RT_g}], \qquad K(T_p) = K_0 \exp[-\frac{E_c}{RT_p}] \tag{33}$$

where, E_c is the effective activation energy for the crystal growth, K_0 is the pre-exponential factor or so-called the frequency factor, and *R* is the universal gas constant (8.314 J/mole.K). The resulting values of these two criteria allusive the tendency of glass to devitrify on heating whereas the glass formation is a kinetic process. The larger their values are the greater the tendency to devitrify. These computations have been carried out in order to compare the stability sequence of the studied material from the quoted parameters with the corresponding sequence computed from stability criteria based on characteristic temperatures. The $K(T_g)$ and $K(T_p)$, as a function of T_g and T_p for the studied alloys are presented in Fig. 10. According to the literature [58, 59], the smaller the values of $K(T_g)$ and $K(T_p)$ criteria, the better should be the glass-forming ability of the material. So the data for both $K(T_g)$ and $K(T_p)$ indicate that the thermal stability decrease with increasing Se content.

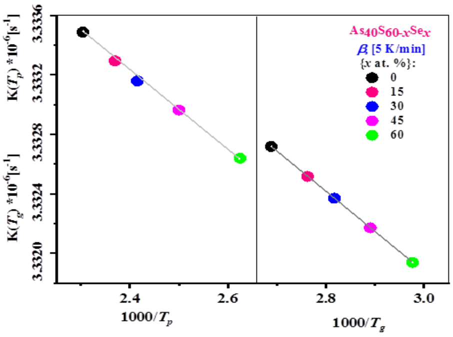

Fig. 10. The plot of $K(T_g)$ *and* $K(T_p)$ *as a function of* T_g *and* T_p *for* $As_{40}S_{60-x}Se_x$
(x = 0, 15, 30, 45 and 60 at. %) alloys at 5 K.min^{-1}*.*

3.11. The iso-conversion methods

3.11.1. Classification of the iso-conversion methods

The principle of iso-conversional states that: "The rates of reaction for the solid state rely only upon the temperatures at constant scope of conversion". According to this principle, the iso-conversion methods and contrast to the non-isothermal methods which implies that both of the Avrami exponent, n and the activation energy E_c should be constant quantities during the transformation process. In contrast, some author's obtain that n and E_c values are not necessarily constant but vary during the transformation process. The variation of the activation energy E_c can be expressed by the local activation energy, E_α. The local activation energy, E_α of amorphous-crystalline transformation can be computed by several iso-conversional models [60]. Iso-conversional methods can be divided into several types on this pattern, (isothermal/non-isothermal), (differential/integral) and (linear/nonlinear). The main reasons for this classification that may be able to change by specific multiples emerging from numerical (differentiation/integration) of temperature integral and then beget similar $E-\alpha$ dependency styles [61].

3.12. Estimation of activation energy

3.12.1. Linear differential iso-conversional Method

The method that proposed by Friedman is a good reliable iso-conversion method because it avoids any mathematical approximations [62]. This method sometimes recognized as transformation rate-isoconversional method, utilized the differential of transformed fraction and thus is named differential iso-conversional method. In our framework, this method has the subsequence general relation:

$$\ln(\varphi)\big|_{\alpha,\beta} = [-\frac{E_\alpha}{RT_{\alpha,\beta}}] + c \tag{34}$$

The plot of, $(\ln(\varphi)|_{\alpha,\beta})$ vs. $(1/T_{\alpha,\beta})$ at a certain values of α accurately requests numerical differentiation. The mentioned plotting should be a straight line whose slope gives us the E_{α} values. Fig. 11 represents the plot of $(\ln(\varphi)|_{\alpha,\beta})$ vs. $(1/T_{\alpha,\beta})$ at 5 K/min and for $\alpha = 0.5$, $\alpha = 0.7$ for the studied samples. The obtained E_{α} values are significantly irregular and equal to 7.126 KJ/ mole for $\alpha = 0.5$ and 5.86 KJ/mole for $\alpha = 0.7$.

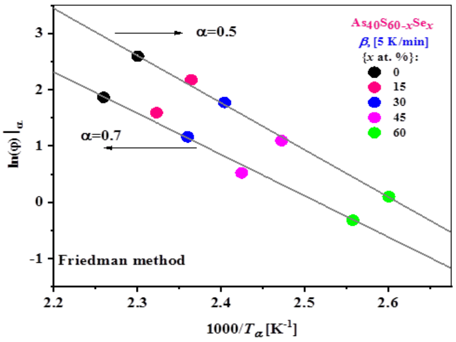

Fig. 11. The plots of $\ln(\varphi)|_{\alpha}$ *versus* $1000/T_{\alpha}$ *T at specific degree of crystallization, α=0.5 and α=0.7 for the studied system.*

3.12.1.1. *Linear integral iso-conversional method*

There are many linear methods and approximations which applied to numerically solve the temperature integral [63], in this work; we will utilize the most popular method, namely, Kissinger-Akahira-Sunose (KAS) method [64], which has the subsequence generalized relation:

$$\ln\left(\frac{\beta}{T_{\alpha}^{2}}\right) = \left[\frac{E_{\alpha}}{RT_{\alpha}}\right] - C \qquad (35)$$

The local activation energy of crystallization E_{α} is computed from the slopes of the resulting straight lines for the plots between $\ln\left(\frac{\beta}{T_{\alpha}^{2}}\right)$ against, $\frac{1000}{T_{\alpha}}$. Fig. 12 represents a graph of the Kissinger equation for different fractional conversion, α where $0.1 \leq \alpha \leq 0.9$ at heating rate equals to 5 K/min^{-1}. The yield values of the local crystallization activation energy E_{α} as function of various degree of conversion, α, are decreased with increasing of degree of conversion as shown in Fig. 13. The behavior of increasing for E_{α} as a function of α can be referred to the breakage of strong linkages of linear chain as a result of increasing Se content in the studied alloys.

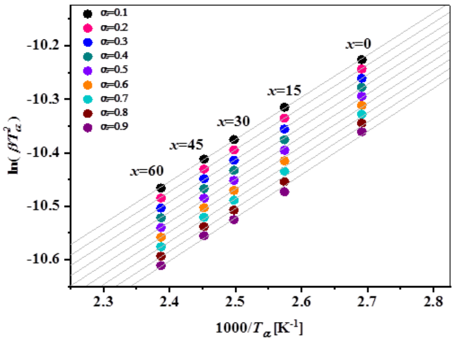

Fig. 12. The plots of $\ln(\beta/T_{\alpha}^{2})$ *versus* $1000/T_{\alpha}$ *T at specific degree of crystallization, α (0.1 to 0.9) for the studied system.*

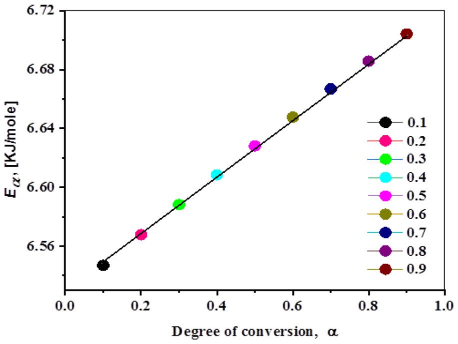

Fig. 13. The plots of the local crystallization activation energy E_α as function of various degree of conversion, α for the studied system.

3.13. The validity of JMA or SB model

To describe the crystallization process, there are two suggested functions $y(\alpha)$ and $z(\alpha)$, which are named the test functions and utilized to test the validity of JMA or SB modal and the two functions are expressed as follows [65]:

$$y(\alpha) = \varphi \exp(-\frac{E_c}{RT}) \tag{36}$$

$$z(\alpha) = \varphi T^2 \tag{37}$$

According to JMA and SB models, the theoretical heat flow, φ is given by the subsequence equation [62]:

$$\varphi = (\Delta H_c).A.\exp[-\frac{E_c}{RT}].f(\alpha) \tag{38}$$

where, ΔH_c is the crystallization enthalpy, A is the pre-exponential frequency factor, E_c is the overall crystallization activation energy, and α, the degree of crystallization or conversion and $f(\alpha)$ is the analytical expression of the kinetic model function. The analytical functions that characteristic the JMA and SB model can be expressed it by the subsequence relations, respectively [66-68]:

$$f(\alpha) = n(1-\alpha)[-\ln(1-\alpha)]^{(n-1)/n} \tag{39}$$

$$f(\alpha) = \alpha^M (1-\alpha)^N \tag{40}$$

Here, the exponent n is related to the nucleation and crystal growth mechanisms whereas M and N are kinetic parameters and denote the relative contribution of acceleratory and decaying regions of the transformation process, respectively.

The JMA model is suitable to describe the crystallization process if the maximum α_p^∞ of the function of $z(\alpha)$ falls into the range of (0.61–0.65) [69]. While SB model can be utilized to describe the thermal analyses if 0 < $\alpha_M < \alpha_p^\infty$, where α_M is maximum of the $y(\alpha)$ function [66]. The $y(\alpha)$ and $z(\alpha)$ functions are normalized within the (0, 1) range, and reach their maxima when α equal to α_M and α_p^∞, respectively, so that ,one can be expressed the two functions as follows:

$$y(\alpha)\Big|_{N\,[0,1]} = \frac{\varphi \exp(-\frac{E_c}{RT})}{Max\,[\varphi \exp(-\frac{E_c}{RT})]}\,, \qquad z(\alpha)\Big|_{N\,[0,1]} = \frac{\varphi T^{2}}{Max\,[\varphi T^{2}]} \tag{41}$$

To determined $y(\alpha)$ function, the average values of $E(\alpha)$ deduced by the iso-conversion method of Kissinger–Akahira–Sunose were utilized. The variations of $y(\alpha)$ and $z(\alpha)$ functions with the fractional conversion are presented in Fig. 14. From the plots of $y(\alpha)$ and $z(\alpha)$ versus α, the values of α_M and α_p^∞ corresponds to their maxima are evaluated and the summarized in Table 4. The obtained values of α_p^∞ and α_M decrease with increasing of Se content in the studied framework as presented in Table 4. As well, the value of α_p^∞ is fall into (0.61-0.65) range for (x=0 at.%) and significantly smaller than the fingerprint of the JMA model for the rest investigated alloys.

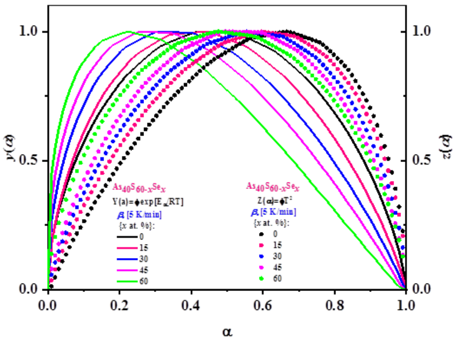

Fig. 14. The variations of $y(\alpha)$ and $z(\alpha)$ normalized functions with the fractional conversion, α for the studied system.

Thus we concluded that the JMA mode is not suitable to study the crystallization kinetics for investigated alloys with (x=15, 30, 45 and 60 at. %) and suitable to study the crystallization kinetics for the first alloy in the studied system. The resulting values of α_p^∞ are lower values than 0.632 indicates a complex and accelerated crystallization process [70]. Such behavior of crystallization could be quantitatively described by the empirical *SB (M, N)* model. The kinetic exponents *M* and *N* are two parameters that define the relative contribution of acceleratory and decay parts of the crystallization process [70]. The *M* and *N* parameters can be computed by α_M values [71] as:

$$\frac{M}{N} = (\frac{\alpha_M}{1-\alpha_M}) \tag{42}$$

According to the average values of *E*, computed by KAS method from Eq. (35) and $\frac{M}{N}$ values computed from Eq. (42), the *N* values are determined via the following equation [71]

$$\ln(\varphi \exp[\frac{E_c}{RT}]) = \ln(\Delta H_C . A) + N\ \ln[\alpha^{\frac{M}{N}}(1-\alpha)] \tag{43}$$

This equation is valid in the interval of 0.2≤ α ≤0.8. The values of *N* could be found from the slopes of the plots of $\ln(\varphi \exp[\frac{E_c}{RT}])$ versus $\ln[\alpha^{\frac{M}{N}}(1-\alpha)]$ as shown in Fig. 15 and the *M* values are computed by Eq. (42) where the value of M is limited to the interval (0, 1). The intersections of these plots are utilized to compute the values of the pre-exponential factor *A* for investigated compositions, where enthalpy (ΔH_C) that describe the non-isothermal crystallization for the studied alloys listed in Table 4.

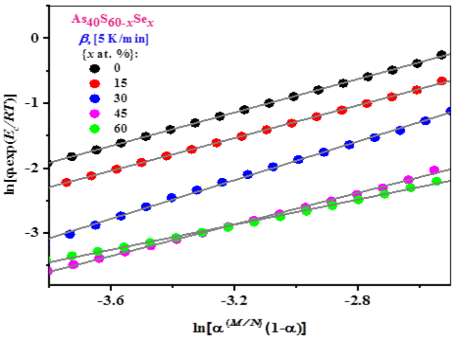

Fig. 15. The plots of $\ln(\varphi\exp[\frac{E_c}{RT}])$ *versus* $\ln[\alpha^{\frac{M}{N}}(1-\alpha)]$ *for the studied system.*

On the other hand, the values of the Avrami exponent *n* and the pre-exponential factor *A* can be computed based on the JMA model by [69]:

$$\left.\begin{aligned} \alpha_M &= 0 && \text{for} \quad n \le 1 \\ \alpha_M &= 1-\exp[n^{-1}-1] && \phantom{\text{for}} \quad n \succ 1 \end{aligned}\right\} \tag{44}$$

Hence, from the kinetic equation for the JMA model, it can be written in the logarithmic form as [72]:

$$\ln(\varphi\exp[\frac{E_C}{RT}]) = \ln(\Delta H_C . A) + \ln\{n(1-\alpha)[-\ln(1-\alpha)]^{\frac{(n-1)}{n}}\} \tag{45}$$

Fig. 16 represents the plots of $\ln(\varphi\exp[\frac{E_C}{RT}])$ versus $\ln\{n(1-\alpha)[-\ln(1-\alpha)]^{\frac{(n-1)}{n}}\}$ for the studied alloys. Table 5 summarizes the parameters (*M, N*), the pre-exponential *A*, α_p^∞, α_M and *n*.

Table 5. Parameters of the normalized functions, SB and JMA model for studied alloys.

x at.%	Max. "$(y(\alpha))$"	Max. "$(z(\alpha))$"	SB		JMA	
	α_M	α_M^∞	N	M	n	A (min^{-1})
0	0.490	0.646	0.789	0.758	3.061	0.78260
15	0.464	0.595	0.753	0.651	2.656	0.74616
30	0.404	0.565	0.734	0.497	2.072	1.21131
45	0.353	0.525	0.727	0.396	1.771	0.49934
60	0.252	0.474	0.695	0.234	1.409	0.65265

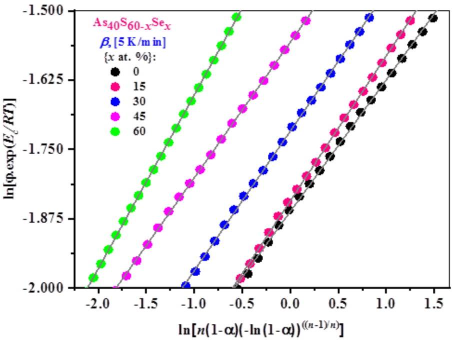

Fig. 16. The plots of $\ln(\varphi \exp[\frac{E_C}{RT}])$ *versus* $\ln\{n(1-\alpha)[-\ln(1-\alpha)]^{\frac{(n-1)}{n}}\}$ *for the studied system.*

3.14. The theatrical DSC curves

In order to test the correctness of local activation energies and local Avrami exponents we computed the theatrical DSC curves according to the SB and JMA models by the mentioned equations in this regard. The deduced theoretical and experimental DSC curves based on JMA and SB models are shown in Fig. 17 and Fig. 18. It is obvious that DSC curves computed via JMA model are not agreement with experimental data in the last four alloys and agreement with the first alloy. On the other hand, the DSC curves computed via SB model as shown in Fig. 18 are agreed with the experimental data at all studied alloys. From the last discussion, we can say that the empirical *SB (M, N)* model is the most suitable model to quantitatively describe the crystallization process in the studied alloys. The JMA model is a specific case of the two-parameter (*M*, *N*) SB kinetic model. It can be show [69] that there are combination of parameters *M* and *N* corresponding to a given value of kinetic exponent for the JMA model (when $n \geq 1$). Therefore, the SB kinetic model can be used for a quantitative description of more complicated phase transformation involving both nucleation and growth.

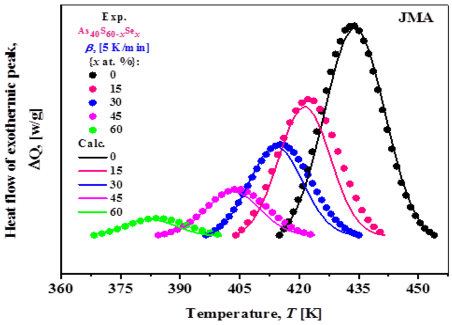

Fig. 17. The computed theoretical DSC curves (solid lines) using JMA model and the experimental DSC curves (solid symbols) for the studied system.

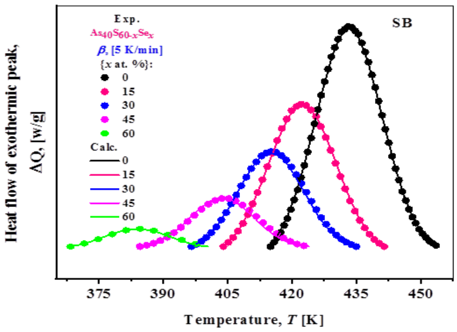

Fig. 18. The computed theoretical DSC curves (solid lines) using SB model and the experimental DSC curves (solid symbols) for the studied system.

3.15. Identification of the crystalline phases by X-ray and SEM analysis

To identify the possible phases that crystallize during the thermal treatment applied to the glassy alloy, the x-ray diffraction patterns of glassy alloy $As_{40}S_{45}Se_{15}$ (as an example about all studied samples) annealed at 370, 390, 400 and 410 K for 0.5 h, which are referred at Fig. 19 (a). For this purpose, Fig. 19 (b) appears the most relevant portions of the diffractometer tracings for the glass (after T_g) and for the material annealed process. Fig. 19 (a) has broad hump being characteristic of the amorphous phase of the starting material at diffraction angles (2θ) between 5^o and 70^o. The presence of one amorphous hump (at 370 K) may be interpreted in terms of the finding of one amorphous phase of glass. The diffractogram of the transformed material after the crystallization process suggests the presence of micro-crystallites of As_2 (Se, S)$_3$ of monoclinic crystal system as dominant phase according to JSTM (No. card: 040-0469) [73] at 410 K as shown in Fig. 19 (a), which were cause the presence of one peak in the DSC traces.. Fig. 19 (a) shows that the intensity of the peaks increases with increasing of annealed temperature, while there remains also a residual amorphous phase. We have confirmed what we saw when examining by utilizing x-rays to prove the amorphous and crystalline state using the electron microscope, namely, SEM photos as shown in Fig. 20. From this figure, one can notice that the size of crystallization increases with increasing of annealed temperature and also the generated crystals take the form similar to a spherical shape.

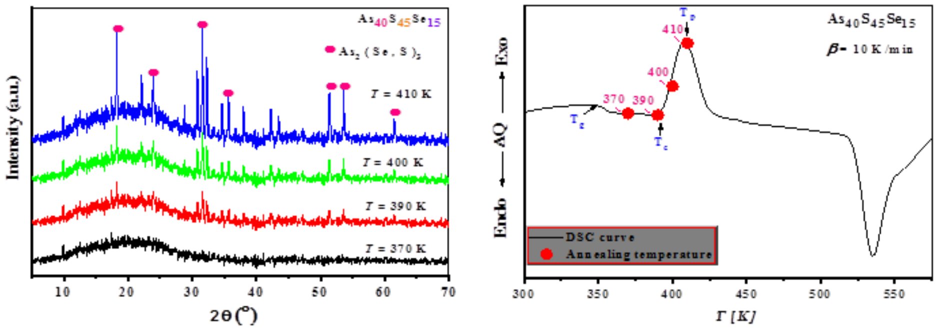

Fig. 19. The plot of annealed temperature according to DSC curve (a) and the plot of x-ray diffraction patterns of $As_{40}S_{45}Se_{15}$ glassy alloy (b) for the studied system.

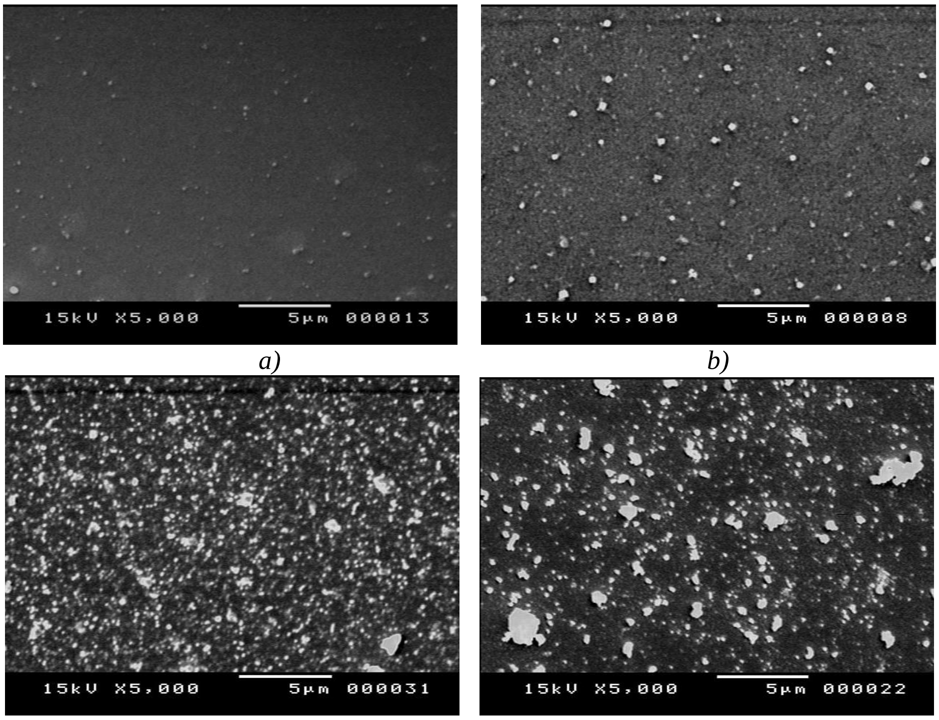

a) *b)*

b) *d)*

Fig. 20 SEM images of surface morpholog of the sample annealed at : a)370 K, b)390 K, c)400 K, d) 410 K

4. Conclusions

In the framework, the chalcogenide of the $As_{40}S_{60-x}Se_x$ glassy alloys, with (x=0, 15, 30, 45 and 60 at. %) are prepared by the melt-quenching technique. Structure parameters for the studied compositions were discussed. Fitting of the kinetic model to isothermal transformation-rate data, as exhibited by DSC scans. The characteristic temperatures (T_g ,T_c ,T_p and T_m) were computed and thus the activation energy for the glass transition, amorphous-crystallization, and crystallization transformations. The crystallization kinetics of the system was investigated by non-isothermal DSC and the values of the activation energy, E_c , and Avrami index, *n*, were computed by Matausita method also the activation energy, E_c was deduced by other non-isothermal and conversional methods, the crystallization activation energy (E_c) is computed by iso-conversion via Friedman and Kissinger methods. The change of value E_c with increasing crystallization conversion factor is attributed to the complex mechanism of the crystallization process. The results appear strong Se content dependence of the activation energy. Avrami exponent, *n*, is closed to 2.31 and 2,97 thus corresponding to complex processes include different mechanisms. On the other hand, the thermal stability for the powdered of studied glassy alloys at t heating rate (5 K/min) has been computed by various criteria. The obtained results of the $K(T_g)$ and $K(T_g)$ agree satisfactorily with other criteria for the studied glassy alloys. The observed data of the thermal stability criteria indicate that the studied glasses are the less stable. The results appear that the conditions of the Sestak–Berggren model are satisfied for describing the crystallization for the studied system.

Acknowledgment

The authors extended their appreciation the Deanship of Scientific Research at King Khalid University (KKU) for funding this research project, Number: (R.G.P2./62/40).

References

[1] R. Zallen, C. M. Penchina, American Journal of Physics **54**, 862 (1986).
[2] A. Burian, P. Lecante, A. Mosset, J. Galy, J. M. Tonnerre, D. Raoux, Journal of non-crystalline solids **212**(1), 23 (1997).
[3] C. Lopez, (2004). Evaluation of the photo-induced structural Mechanisms in chalcogenide glass materials (Doctoral dissertation, University of Central Florida).
[4] S. S. Flaschen, A. D. Pearson, W. R. Northover, Journal of the American Ceramic Society **42**(9), 450 (1959).
[5] A. K. Singh, Chalcogenide Letters **8**(2), 123 (2011).
[6] A. K. Singh, N. Mehta, K. Singh, Philosophical magazine letters **90**(3), 201 (2010).
[7] A Goel, E. R. Shaaban, M. J. Ribeiro, F..C..L. Melo, J. M. F. Ferreira. Journal of Physics: Condensed Matter **19** (38), 386231 (2007)
[8] H. Peng, Z. Liu, Coordination Chemistry Reviews **254**(9-10), 1151 (2010).
[9] T. Velinov, M. Gateshki, D. Arsova, E. Vateva, Physical Review B **55**(17), 11014 (1997).
[10] C. Y. Yang, M. A. Paesler, D. E. Sayers, Physical Review B **39**(14), 10342 (1989).
[11] V. Vassilev, K. Tomova, V. Parvanova, S. Boycheva, Journal of alloys and compounds **485**(1-2), 569 (2009).
[12] J. B. Wachter, K. Chrissafis, V. Petkov, C. D. Malliakas, D. Bilc, T. Kyratsi, M. G. Kanatzidis, Journal of Solid State Chemistry **180**(2), 420 (2007).
[13] V. G. Ta'eed, N. J. Baker, L. Fu, K. Finsterbusch, M. R. Lamont, D. J. Moss, B. Luther-Davies, Optics Express **15**(15), 9205 (2007).
[14] E. R. Shaaban, M. Y. Hassaan, M. G. Moustafa, A. Qasem, G. A. Ali, Optik **186**, 275 (2019).

[15] E. R. Shaaban, M. Y. Hassaan, M. G. Moustafa, A. Qasem, G. A. M. Ali, E. S. Yousef, Acta Physica Polonica A **136**(3), 2019.
[16] E. R. Shaaban, M. Y. Hassaan, M. G. Moustafa, A. Qasem, Applied Physics A **126**(1), 34 (2020).
[17] A. F. Ioffe, A. R. Regel, Prog. Semicond. **4**(89), 237 (1960).
[18] A. Zakery, S. R. Elliott, Journal of Non-Crystalline Solids **330**(1-3), 1 (2003).
[19] E. R. Shaaban, MY Hassaan, AG Mostafa, AM Abdel-Ghany (2009), Journal of alloys and compounds **482** (1-2), 440 (2009).
[20] A. Goel, E. R. Shaaban, D. U. Tulyaganov, J. M. F. Ferreira, Journal of the American Ceramic Society **91** (8), 2690 (2008).
[21] L. Zhenhua, Journal of non-crystalline solids **127**(3), 298 (1991).
[22] L. Tichý, H. Ticha, Journal of Non-Crystalline Solids **189**(1-2), 141 (1995).
[23] J. H. Schachtschneider, R. G. Snyder, Spectrochimica Acta **19**(1), 117 (1963).
[24] L. Pauling, (1960), The Nature of the Chemical Bond, (Vol. 260, pp. 3175-3187). Ithaca, NY: Cornell university press.
[25] S. R. Elliott, Physics of amorphous materials. Longman Group, Longman House, Burnt Mill, Harlow, Essex CM 20 2 JE, England, 1983.
[26] T. T. Nang, M. Okuda, T. Matsushita, Physical Review B **19**(2), 947 (1979).
[27] Z. Sun, J. Zhou, R. Ahuja, Physical review letters **98**(5), 055505 (2007).
[28] J. Bicerano, S. R. Ovshinsky, J. Non-Cryst. Solids **74**, 141 (1985).
[29] R. Sathyamoorthy, J. Dheepa, Journal of Physics and Chemistry of Solids **68**(1), 111 (2007).
[30] S. A. Fayek, Infrared physics & technology **46**(3), 193 (2005).
[31] H. A. El Ghani, M. A. El Rahim, M. M. Wakkad, A. A. Sehli, N. Assraan, Physica B: Condensed Matter **381**(1-2), 156 (2006).
[32] S. A. Fayek, M. R. Balboul, K. H. Marzouk, Thin Solid Films **515**(18), 7281 (2007).
[33] E. R. Shaaban, M. M. Soraya, M. Shapaan, H. S. Hassan, M. M. Samar, Journal of Alloys and Compounds **693**, 1052 (2017).
[34] M. F. Thorpe, Journal of Non-Crystalline Solids **57**(3), 355 (1983).
[35] R. T. Sanderson, (1971), Inorganic Chemistry (New Delhi: Affiliated East.
[36] W. Kauzmann, Chemical reviews **43**(2), 219 (1948).
[37] D. Turnbull, Contemporary physics **10**(5), 473 (1969).
[38] S. Mahadevan, A. Giridhar, A. K. Singh, Journal of non-crystalline solids **88**(1), 11 (1986).
[39] A. R. Ma, A. El-Korashy, S. Al-Ariki, Materials transactions **51**(2), 256 (2010).
[40] N. Afify, M. A. Abdel-Rahim, A. A. El-Halim, M. M. Hafiz, Journal of non-crystalline solids **128**(3), 269 (1991).
[41] S. Mahadevan, A. Giridhar, Journal of non-crystalline solids **197**(2-3), 219 (1996).
[42] M. Saad, M. Poulin, Mater. Sci. Forum **19-20**, 11 (1987).
[43] A. Hrubý, Czechoslovak Journal of Physics B **22**(11), 1187 (1972).
[44] K. Shimakawa, Journal of Non-Crystalline Solids **43**(2), 229 (1981).
[45] H. E. Kissinger, Analytical chemistry **29**(11), 1702 (1957).
[46] M. A. Abdel-Rahim, A. Y. Abdel-Latif, A. El-Korashy, G. A. Mohamed, Journal of materials science **30**(22), 5737 (1995).
[47] J. Vázquez, C. Wagner, P. Villares, R. Jiménez-Garay, Acta materialia **44**(12), 4807 (1996).
[48] K. Chebli, J. M. Saiter, J. Grenet, A. Hamou, G. Saffarini, Physica B: Condensed Matter **304**(1-4), 228 (2001).
[49] M. M. Wakkad, E. K. Shokr, S. H. Mohamed, Journal of non-crystalline solids **265**(1-2), 157 (2000).
[50] G. M. Bartenev, In Dokl. Akad. Nauk SSSR **76**(2), 227 (1951).
[51] I. Gutzow, J. Schmelzer, (1995), The Vitreous State Berlin.
[52] P. G. Debenedetti, (1996), Metastable liquids: concepts and principles, Princeton University Press.
[53] P. Duhaj, D. Barančok, A. Ondrejka, Journal of Non-Crystalline Solids **21**(3), 411 (1976).
[54] K. Tanaka, Physical Review B **39**(2), 1270 (1989).
[55] K. Matusita, T. Komatsu, R. Yokota, Journal of Materials Science **19**(1), 291 (1984).
[56] S. Surinach, M. D. Baro, M. T. Clavaguera-Mora, N. Clavaguera, Journal of materials science

19(9), 3005 (1984).

[57] L. Hu, Z. Jiang, Chin J. A new criterion for crystallization of glass. Ceram Soc. **18**, 315 (1990).

[58] J. Vazquez, P. L. Lopez-Alemany, P. Villares, R. Jimenez-Garay, Journal of alloys and compounds **354**(1-2), 153 (2003).

[59] E. R. Shaaban, M. Shapaan, Y. B. Saddeek, Journal of Physics: Condensed Matter **20**(15), 155108 (2008).

[60] T. Akahira, T. Sunose, Res. Report Chiba Inst. Technol. Sci. Technol. **16**, 22 (1971).

[61] J. H. Flynn, Thermochimica Acta **300**(1-2), 83 (1997).

[62] H. L. Friedman, Journal of Polymer Science Part B: Polymer Letters **7**(1), 41 (1969).

[63] S. Vyazovkin, A. K. Burnham, J. M. Criado, L. A. Pérez-Maqueda, C. Popescu, N. Sbirrazzuoli, Thermochimica acta **520**(1-2), 1 (2011).

[64] C. Păcurariu, R. Lazău, I. Lazău, R. Ianoş, B. Ţiţa, Journal of thermal analysis and calorimetry **97**(2), 507 (2009).

[65] J. Málek, Thermochimica Acta **355**(1-2), 239 (2000).

[66] J. Šesták, G. Berggren, Thermochimica Acta **3**(1), 1 (1971).

[67] J. D. Hancock, J. H. Sharp, Journal of the American Ceramic Society **55**(2), 74 (1972).

[68] J. H. Schachtschneider, R. G. Snyder, Spectrochimica Acta **19**(1), 117 (1963).

[69] J. Málek, Thermochimica acta **267**, 61 (1995).

[70] M. Marinović-Cincović, B. Janković, B. Milićević, Ž.Antić, R. K. Whiffen, M. D. Dramićanin, Powder technology **249**, 497 (2013).

[71] P. Pustkova, D. Švadlák, J. Shánělová, J. Málek, Thermochimica acta **445**(2), 116 (2006).

[72] H. L. Friedman, (1964). Kinetics of thermal degradation of char-forming plastics from thermogravimetry, Application to a phenolic plastic. In Journal of polymer science part C: polymer symposia (Vol. 6, No. 1, pp. 183-195). New York: Wiley Subscription Services, Inc., A Wiley Company.

[73] P. J. Dunn, D. R. Peacor, A. J. Criddle, R. B. Finkelman, Mineralogical Magazine **50**(356), 279 (1986).